

CISS effect

Magnetocurrent-voltage characteristics with Coulomb interactions. II

Huisman, K. H.; Heinisch, J. B.M.Y.; Thijssen, J. M.

DOI

[10.1063/5.0148748](https://doi.org/10.1063/5.0148748)

Publication date

2023

Document Version

Final published version

Published in

Journal of Chemical Physics

Citation (APA)

Huisman, K. H., Heinisch, J. B. M. Y., & Thijssen, J. M. (2023). CISS effect: Magnetocurrent-voltage characteristics with Coulomb interactions. II. *Journal of Chemical Physics*, 158(17), Article 174108. <https://doi.org/10.1063/5.0148748>

Important note

To cite this publication, please use the final published version (if applicable). Please check the document version above.

Copyright

Other than for strictly personal use, it is not permitted to download, forward or distribute the text or part of it, without the consent of the author(s) and/or copyright holder(s), unless the work is under an open content license such as Creative Commons.


Takedown policy

Please contact us and provide details if you believe this document breaches copyrights. We will remove access to the work immediately and investigate your claim.

RESEARCH ARTICLE | MAY 02 2023

CISS effect: Magnetocurrent–voltage characteristics with Coulomb interactions. II

Special Collection: [Chiral Induced Spin Selectivity](#)

K. H. Huisman  ; J. B. M. Y. Heinisch ; J. M. Thijssen



J. Chem. Phys. 158, 174108 (2023)

<https://doi.org/10.1063/5.0148748>



View
Online



Export
Citation

CrossMark

Articles You May Be Interested In

Studies of carrier recombination in solution-processed $\text{CuIn}(\text{S},\text{Se})_2$ through photoluminescence spectroscopy

Appl. Phys. Lett. (February 2013)

Characterization of total ionizing dose damage in COTS pinned photodiode CMOS image sensors

AIP Advances (March 2016)

Theoretical and experimental study of the dark signal in CMOS image sensors affected by neutron radiation from a nuclear reactor

AIP Advances (December 2017)



Time to get excited.
Lock-in Amplifiers – from DC to 8.5 GHz

[Find out more](#)

 Zurich
Instruments

CISS effect: Magnetocurrent-voltage characteristics with Coulomb interactions. II

Cite as: J. Chem. Phys. 158, 174108 (2023); doi: 10.1063/5.0148748

Submitted: 2 March 2023 • Accepted: 18 April 2023 •

Published Online: 2 May 2023



View Online



Export Citation



CrossMark

K. H. Huisman,^{a)} J. B. M. Y. Heinisch, and J. M. Thijssen

AFFILIATIONS

Kavli Institute of Nanoscience, Delft University of Technology, 2628 CJ Delft, The Netherlands

Note: This paper is part of the JCP Special Topic on Chiral Induced Spin Selectivity.

^{a)} Author to whom correspondence should be addressed: k.h.huisman@tudelft.nl

ABSTRACT

One of the manifestations of chirality-induced spin selectivity is the appearance of a magnetocurrent. Magnetocurrent is defined as the difference between the charge currents at finite bias in a two terminal device for opposite magnetizations of one of the leads. In experiments on chiral molecules assembled in monolayers the magnetocurrent is dominantly odd in bias voltage, while theory often yields an even one. From theory it is known that the spin-orbit coupling and chirality of the molecule can only generate a finite magnetocurrent in the presence of interactions, either of the electrons with vibrational modes or among themselves, through the Coulomb interaction. Here we analytically show that the magnetocurrent in bipartite-chiral structures mediated through Coulomb interactions is exactly even in the wide band limit and exactly odd for semi-infinite leads due to the bipartite lattice symmetry of the Green's function. Our numerical results confirm these analytical findings.

© 2023 Author(s). All article content, except where otherwise noted, is licensed under a Creative Commons Attribution (CC BY) license (<http://creativecommons.org/licenses/by/4.0/>). <https://doi.org/10.1063/5.0148748>

I. INTRODUCTION

One of the manifestations of chirality-induced spin selectivity (CISS) is the appearance of a magnetocurrent. Magnetocurrent is defined as the difference between the charge currents at finite bias in a two terminal device for opposite magnetizations of one of the leads. The Onsager-Casimir reciprocity¹⁻³ prohibits a magnetocurrent from being observed in two-terminal junctions in the linear regime. In fully coherent two-terminal transport, this absence of a magnetocurrent extends to the nonlinear regime as well; this is called Büttiker reciprocity.⁴ In order to see a magnetocurrent in the nonlinear regime, coherence must be broken; this is done through interactions of the electrons with vibrational modes or among themselves, through the Coulomb interaction. It should be noted that several experiments⁵⁻⁹ seem to show violation of the Onsager-Casimir reciprocity for reasons that are not yet known. In some of these experiments, the currents for positive and negative magnetization show a plateau of zero current around zero bias voltage such that the demonstration of the Onsager-Casimir reciprocity is not really convincing.

In this paper, we focus on the symmetry of the magnetocurrent vs bias voltage. In two-terminal transport experiments on

chiral molecules, the magnetocurrent is dominantly odd in bias voltage⁵⁻¹⁷ (for an extensive overview, see Ref. 18). In theory, an even magnetocurrent is found by introducing a decoherence node¹⁹ or via the Büttiker voltage probe method.²⁰ A model including spin-dependent, electron-phonon coupling²¹ yields an odd magnetocurrent. However, the seemingly linear magnetocurrent found in Ref. 21 violates the Onsager-Casimir reciprocity. In our previous paper on Coulomb interactions,²² we found that Onsager-Casimir reciprocity is satisfied, and the odd magnetocurrent is mediated by the strong Coulomb interactions, in combination with the next nearest-neighbor, spin-orbit coupling, making the lattice non-bipartite. We found, in the wide-band limit (WBL), that the magnetocurrent was nearly perfectly odd in the bias voltage, when the Fermi level was aligned with the energy around which the spectrum is approximately particle-hole symmetric. In this paper, we study the bias dependence of the magnetocurrent for a bipartite lattice when the Fermi level is aligned with the energy around which the spectrum is exactly particle-hole symmetric. We show that, close to this symmetry point, there is a difference between the bias dependence of the magnetocurrent for bipartite and non-bipartite lattices.

In most work done on two-terminal transport through molecular junctions, the leads are modeled using the wide-band limit

(see, e.g., Refs. 19–22); however, for some metals, semi-infinite (SIF) leads may be more realistic. We will analyze the magnetocurrent analytically for the WBL and SIF leads by exploiting the bipartite lattice symmetry and the time reversal property of the Green's function. To confirm our analytical findings, we analyze a chiral model system with a nearest-neighbor spin-orbit coupling and Coulomb interactions numerically.

In Sec. II, we define our model. In Sec. III, the magnetocurrent is analyzed analytically for the WBL and SIF leads. In Sec. III A, we define the magnetocurrent, in Sec. III B, we define the Green's functions in the Hartree-Fock (HFA) and Hubbard One approximation (HIA), and in Sec. III C, it is specified how these Green's functions transform under bipartite lattice symmetry and the time-reversal operator. In Secs. III D and III E, the bias dependence of the magnetocurrent is analyzed for the WBL and SIF leads, respectively, in Sec. IV the numerical results are presented, and we conclude our work in Sec. V.

II. MODEL DESCRIPTION

The Hamiltonian of a molecular transport junction is given by

$$\mathbf{H} = \mathbf{H}_{\text{os}} + \mathbf{H}_{\text{T}} + \mathbf{H}_{\text{SOC}} + \mathbf{H}_{\text{U}} + \mathbf{H}_{\text{lead-molecule}} + \mathbf{H}_{\text{leads}}, \quad (1)$$

where \mathbf{H}_{os} is the on-site Hamiltonian, \mathbf{H}_{T} is the hopping Hamiltonian, \mathbf{H}_{SOC} is the hopping Hamiltonian due to spin-orbit coupling, \mathbf{H}_{U} describes the Coulomb interactions, $\mathbf{H}_{\text{lead-molecule}}$ describes the coupling of the molecule to the leads, and $\mathbf{H}_{\text{leads}}$ describes the Hamiltonian of the leads. The onsite Hamiltonian is given by $\mathbf{H}_{\text{os}} = \sum_m \varepsilon_m \hat{n}_m$; we set this to zero ($\varepsilon_m = 0$) throughout this paper. The hopping Hamiltonian is given by $\mathbf{H}_{\text{T}} = -\sum_m t \hat{c}_{m+1}^\dagger \hat{c}_m + \text{h.c.}$, where t is the hopping parameter, and h.c. denotes the Hermitian conjugate. In order to see the effect of bipartite lattice symmetry, we consider an S-shaped structure,²³ see Fig. 1. The spin-dependent hopping Hamiltonian acting between the nearest neighbor sites is given by

$$\mathbf{H}_{\text{SOC}} = -i\lambda \sum_k \sum_{\langle m,n \rangle} \hat{c}_m^\dagger \boldsymbol{\sigma} \cdot (\mathbf{e} \times \mathbf{d}_k) \hat{c}_n + \text{h.c.}, \quad (2)$$

with λ being the spin-orbit coupling parameter. A constant electric field pointing in the out-of-plane direction generates this nearest-neighbor, spin-dependent hopping, and the components of $\boldsymbol{\sigma}$ are the Pauli-matrices. Here \mathbf{d}_k is the hopping vector, k indicates its direction (longitudinal and transverse), and \mathbf{e} indicates the direction of the electric field. This model is defined on a 2D lattice, where the

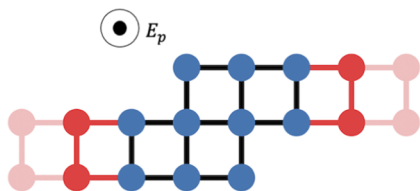


FIG. 1. Schematic of the S geometry. Blue dots are sites of the scattering region, and the red dots are sites on the lead. The black and red links between the sites represent hopping. E_p is the component of the electric field pointing in the out-of-plane direction.

indices m, n label the sites. \mathbf{H}_{U} contains the Coulomb interactions; we take those to be on-site:

$$\mathbf{H}_{\text{U}} = U \sum_m \left(\hat{n}_{m\uparrow} - \frac{1}{2} \right) \left(\hat{n}_{m\downarrow} - \frac{1}{2} \right). \quad (3)$$

Here, U is the Coulomb interaction strength. The factors of $\frac{1}{2}$ are included to make the spectrum of the Hamiltonian particle-hole symmetric around the energy $\varepsilon = 0$. The S-shape in Fig. 1 has a C_2 symmetry around the out-of-plane direction p , leading to a difference between the (non-spin flip) spin-up and down transmissions.²³ Here, $\mathbf{H}_{\text{lead-molecule}}^\alpha = \sum_{k,m,s,s'} V_{ms,ks'}^\alpha c_{ms}^\dagger a_{ks'}^\alpha + \text{h.c.}$, where $V_{ms,ks'}^\alpha$ is the coupling parameter between electrons on the molecule and lead α . The Hamiltonian of the non-interacting lead α is $\mathbf{H}_{\text{lead}}^\alpha = \sum_{k,s} \varepsilon_{ks}^\alpha a_{ks}^\dagger a_{ks}^\alpha$.

III. THEORY

A. Magnetocurrent definition

The transmission for a two-terminal system with Coulomb interactions depends on the bias voltage V through the electron densities: $T_{\text{LR}}(\varepsilon, m) \rightarrow T_{\text{LR}}(\varepsilon, m, V) = T_{\text{LR}}(\varepsilon, m, \langle n_{ks}(m, V) \rangle)$, where $\langle n_{ks}(m, V) \rangle$ is the average electron density for site k with spin s , given by Eq. (14), and m is the magnetization of the left lead. The current into the left lead is then given by (see Appendix F)

$$I(m, V) = \frac{e}{h} \int_{-\infty}^{\infty} T_{\text{LR}}(\varepsilon, m, V) (f(\varepsilon, \mu_L) - f(\varepsilon, \mu_R)) d\varepsilon, \quad (4)$$

where $f(\varepsilon, \mu_\alpha) = [\exp(\beta_\alpha(\varepsilon - \mu_\alpha)) + 1]^{-1}$, μ_α is the chemical potential of lead α , and $\beta_\alpha = \frac{1}{k_B T_\alpha}$, with T_α the temperature of lead α . We will restrict ourselves to equal temperatures for the leads $\beta_{L,R} = \frac{1}{k_B T} = \beta$. The chemical potential of the left and right leads read are given by $\mu_L = E_F + \frac{1}{2}V$, $\mu_R = E_F - \frac{1}{2}V$ (assuming symmetric capacitive coupling). The transmission is given by

$$T_{\text{LR}}(\varepsilon, m, V) = \text{Tr} [\Gamma_L(\varepsilon, m) \mathbf{G}^+ \Gamma_R(\varepsilon) \mathbf{G}^-(\varepsilon, \langle n_{ks}(m, V) \rangle, m)]. \quad (5)$$

Note that from now on, whenever a product of operators occurs, the arguments of the Green's functions are written at the end of the product; so, in Eq. (5), the retarded and advanced Green's functions depend on the same argument $(\varepsilon, \langle n_{ks}(m, V) \rangle, m)$. It can be seen that we only magnetize the left lead with magnetization m . Using Eq. (4), we can write the magnetocurrent as

$$\begin{aligned} \Delta I(m, V) &\equiv I(m, V) - I(-m, V) \\ &= \int_{-\infty}^{\infty} [T_{\text{LR}}(\varepsilon, m, V) - T_{\text{LR}}(\varepsilon, -m, V)] \\ &\quad \times (f(\varepsilon, \mu_L) - f(\varepsilon, \mu_R)) d\varepsilon. \end{aligned} \quad (6)$$

It is our goal to determine the bias dependence of the magnetocurrent $\Delta I(m, V)$. If the Coulomb interactions are absent ($U = 0$), the magnetocurrent vanishes due to Büttiker's reciprocity theorem for two-terminal systems. Thus, we should go beyond the non-interacting particle picture ($U \neq 0$) in order to find a finite magnetocurrent, in the presence of spin-orbit coupling.^{20,22,24} This magnetocurrent can only be non-linear in the bias voltage, since the linear terms vanish due to the Onsager-Casimir reciprocity¹⁻³ theorem. Due to the absence of vibrational modes in our description, only the Coulomb interactions can be responsible for the occur-

rence of a non-zero magnetocurrent, and these interactions manifest themselves through the electron densities. The bias dependence of the magnetocurrent, therefore, has its origin in the bias dependence of the electron densities. We study the bias dependence of the electron densities in detail by exploiting the bipartite lattice symmetry and time-reversal property of the Green's function.

B. Electron Green's function

The retarded Green's function of the scattering region, coupled to leads, in the Hartree–Fock approximation is given by

$$\mathbf{G}_{\text{HFA}}^+(\varepsilon, \langle n_{k_s}(m, V) \rangle, m) = \left[\left(\varepsilon + \frac{U}{2} \right) \mathbf{I} - \mathbf{H}_{\text{T}} - \mathbf{H}_{\text{SOC}} - U \mathbf{n}(\langle n_{k_s}(m, V) \rangle) - \Sigma(\varepsilon, m) \right]^{-1}, \quad (7)$$

and, in the Hubbard One approximation, the retarded Green's function is given by (see, e.g., Chap. 12 of Haug and Jauho²⁵)

$$\mathbf{G}_{\text{HIA}}^+(\varepsilon, \langle n_{k_s}(m, V) \rangle, m) = \left[\left[\left(\varepsilon - \frac{U}{2} \right) \mathbf{I} + U \mathbf{n}(\langle n_{k_s}(m, V) \rangle) \right]^{-1} \times \left(\varepsilon - \frac{U}{2} \right) \left(\varepsilon + \frac{U}{2} \right) \mathbf{I} - \mathbf{H}_{\text{T}} - \mathbf{H}_{\text{SOC}} - \Sigma(\varepsilon, m) \right]^{-1}. \quad (8)$$

For our analyses of the WBL and SIF leads, we will only magnetize the left lead with magnetization m . Here the retarded self-energy is defined as the sum of retarded self-energies for the left and right leads $\Sigma(\varepsilon, m) = \Sigma^{\text{L}}(\varepsilon, m) + \Sigma^{\text{R}}(\varepsilon)$, and the diagonal matrix $\mathbf{n}(\langle n_{k_s}(m, V) \rangle)$ has elements $n_{k_s, k' s'} = \langle n_{k_s}(m, V) \rangle \delta_{k k'} \delta_{s s'}$ (where \bar{s} denotes that spin s is flipped).

In the WBL, the retarded self-energy is purely imaginary and energy-independent; it is given by $\Sigma_{\text{WBL}}(\varepsilon, m) = -\frac{i}{2}(\Gamma_{\text{L}}(m) + \Gamma_{\text{R}})$. Only the diagonal matrix elements of lead α that are coupled to the molecule are nonzero, and they are given by $\gamma_{\alpha}(\mathbf{I} + p_z^{\alpha} \sigma_z)$. Here, γ_{α} is the coupling strength, and $p_z^{\alpha} \in [-1, 1]$ is the magnetic polarization of lead α .

For SIF leads with onsite energy ε_0 and nearest neighbor hopping t_{lead} , the retarded self-energy is given by $\Sigma(\varepsilon) = \Lambda(\varepsilon) - \frac{i}{2}\Gamma(\varepsilon)$. Here, $\Lambda(\varepsilon)$, $\Gamma(\varepsilon)$ are both real and for $|\varepsilon - \varepsilon_0| < 2t_{\text{lead}}$, they are given by²⁶ $\Gamma(\varepsilon, \varepsilon_0, t_{\text{lead}}) = \sqrt{(2t_{\text{lead}})^2 - (\varepsilon - \varepsilon_0)^2}$, $\Lambda(\varepsilon, \varepsilon_0, t) = \frac{\varepsilon - \varepsilon_0}{2}$ and for $|\varepsilon - \varepsilon_0| \geq 2t_{\text{lead}}$, they are given by $\Gamma(\varepsilon, \varepsilon_0, t_{\text{lead}}) = 0$, $\Lambda(\varepsilon, \varepsilon_0, t_{\text{lead}}) = \frac{\varepsilon - \varepsilon_0}{2} - \text{sign}(\varepsilon - \varepsilon_0) \frac{1}{2} \sqrt{(\varepsilon - \varepsilon_0)^2 - (2t_{\text{lead}})^2}$.

For semi-infinite leads, we take the coupling parameter between electrons on the molecule and the lead to be a constant real number, t_c , and, as a consequence, the retarded self-energy is given by $\Sigma(\varepsilon, \varepsilon_0, t_{\text{lead}}) \rightarrow \tilde{\Sigma}(\varepsilon, \varepsilon_0, t_{\text{lead}}, t_c) = \left| \frac{t_c}{t_{\text{lead}}} \right|^2 \left[\Lambda(\varepsilon, \varepsilon_0, t_{\text{lead}}) - \frac{i}{2}\Gamma(\varepsilon, \varepsilon_0, t_{\text{lead}}) \right]$. When lead α is magnetically polarized with $p_z^{\alpha} \in [-1, 1]$, the bands for up and down spin electron split such that for the spin-up bands, $\varepsilon_0 \rightarrow \varepsilon_u = \varepsilon_0 + m^{\alpha}$, and for the spin-down bands, $\varepsilon_0 \rightarrow \varepsilon_d = \varepsilon_0 - m^{\alpha}$, where the magnetization of lead α is defined as $m^{\alpha} = 2t_{\text{lead}} p_z^{\alpha}$. For a SIF lead, magnetized with magnetization m and $\varepsilon_0 = 0$, Γ and Λ satisfy

$$\Gamma(\varepsilon, m) = \Gamma(-\varepsilon, -m), \quad (9)$$

$$\Lambda(\varepsilon, m) = -\Lambda(-\varepsilon, -m). \quad (10)$$

Throughout our analyses for SIF leads, we take the onsite energies of the left and right leads to be zero $\varepsilon_0 = 0$.

C. Green's function: Transformation under time-reversal–And sub-lattice symmetry

The time reversal operator is given by $\mathbf{T} = i\sigma_y \mathbf{K}$, where \mathbf{K} is the conjugation operator. Under \mathbf{T} , the retarded and advanced Green's functions (indicated with a plus and minus, respectively), transform as follows:

$$\mathbf{T} \mathbf{G}^{\pm}(\varepsilon, \langle n_{k_s}(m, V) \rangle, m) \mathbf{T}^{-1} = \mathbf{G}^{\mp}(\varepsilon, \langle n_{k_{\bar{s}}}(m, V) \rangle, -m). \quad (11)$$

We emphasize that in Eq. (11), the magnetization m in the argument of the electron densities does not change sign because the real-valued electron densities transform under \mathbf{T} as $\mathbf{T} \langle n_{k_s}(m, V) \rangle \mathbf{T}^{-1} = \langle n_{k_{\bar{s}}}(m, V) \rangle$.

If the lattice of the system can be separated into sub-lattices A and B such that there is only hopping possible from site A to site B and vice versa, then the system is bipartite. In that case, the Green's function [HFA Eq. (7) and HIA Eq. (8)] in the wide-band limit and for semi-infinite (SIF) leads satisfy

$$\mathbf{G}_{\text{WBL}}^{\pm}(\varepsilon, \langle n_{k_s}(m, V) \rangle, m) = -\mathbf{M} \mathbf{G}_{\text{WBL}}^{\mp}(-\varepsilon, 1 - \langle n_{k_s}(m, V) \rangle, m) \mathbf{M}, \quad (12)$$

$$\mathbf{G}_{\text{SIF}}^{\pm}(\varepsilon, \langle n_{k_s}(m, V) \rangle, m) = -\mathbf{M} \mathbf{G}_{\text{SIF}}^{\mp}(-\varepsilon, 1 - \langle n_{k_s}(m, V) \rangle, -m) \mathbf{M}. \quad (13)$$

Here, \mathbf{M} is a diagonal matrix, which takes the values $+1$ for sites on sublattice A and -1 for sites on sublattice B. Here, the diagonal matrices \mathbf{I} , \mathbf{n} , Σ are invariant under \mathbf{M} , and the nearest neighbor hopping matrices change sign under \mathbf{M} : $\mathbf{M} \mathbf{H}_{\text{T, SOC}} \mathbf{M} = -\mathbf{H}_{\text{T, SOC}}$. Note that particles and holes are interchanged: $\langle n_{k_s}(m, V) \rangle \rightarrow 1 - \langle n_{k_s}(m, V) \rangle$, and note that (contrary to WBL leads) for SIF leads, the magnetization m changes sign under this transformation due to properties of the self-energies in Eqs. (9) and (10) (see Appendix A).

The electron density for site k with spin s is given by

$$\langle n_{k_s}(m, V) \rangle = \int (\mathbf{G}^+ \Gamma^<(\varepsilon, m, V) \mathbf{G}^-(\varepsilon, \langle n_{k_s}(m, V) \rangle, m))_{k_s, k_s} \frac{d\varepsilon}{2\pi}, \quad (14)$$

where (with $E_{\text{F}} = 0$)

$$\Gamma^<(\varepsilon, m, V) = \Gamma_{\text{L}}(\varepsilon, m) f\left(\varepsilon, \frac{V}{2}\right) + \Gamma_{\text{R}}(\varepsilon) f\left(\varepsilon, -\frac{V}{2}\right). \quad (15)$$

Note that in Eq. (14), both the retarded and advanced Green's functions depend on the same argument $(\varepsilon, \langle n_{k_s}(m, V) \rangle, m)$, written at the end of the expression, while $\Gamma^<$ depends on (ε, m, V) . Note that the the Fermi level E_{F} is precisely aligned with the energy $\varepsilon = 0$ around which the density of states, corresponding to these systems, is particle–hole symmetric. This alignment forms one of the cornerstones of our analyses, the other one being that the capacitive coupling to the left and right lead is symmetric.

D. Wide band limit

The wide band limit is representative for a gold lead, with its flat density of states around the Fermi level.²⁷ In

this section, we analyze the electron density in Eq. (14) and the magnetocurrent (6) using the time-reversal and bipartite lattice transformations of the Green's functions in Eqs. (11) and (12). From the time-reversal transformation of the Green's function (11), $\mathbf{T}\langle n_{k\bar{s}}(m, V) \rangle \mathbf{T}^{-1} = \langle n_{k\bar{s}}(m, V) \rangle$ (note that m does not change sign, since \mathbf{T} only flips the spin index of the matrix) follows the identity $\mathbf{G}^+ \mathbf{T}^<(\varepsilon, m, V) \mathbf{G}^-(\varepsilon, \langle n_{k\bar{s}}(m, V) \rangle, m) = \mathbf{T}^{-1} \mathbf{G}^- \mathbf{T}^<(\varepsilon, -m, V) \mathbf{G}^+(\varepsilon, \langle n_{k\bar{s}}(m, V) \rangle, -m) \mathbf{T}$, which we use to rewrite the RHS of Eq. (14). We then multiply both sides from the left with \mathbf{T} and from the right with \mathbf{T}^{-1} , which flips the spin on the LHS and cancels the time-reversal operators on the RHS. Equation (14) then becomes

$$\langle n_{k\bar{s}}(m, V) \rangle = \int_{-\infty}^{\infty} (\mathbf{G}^- \mathbf{T}^<(\varepsilon, -m, V) \mathbf{G}^+(\varepsilon, \langle n_{k\bar{s}}(m, V) \rangle, -m))_{ks,ks} \frac{d\varepsilon}{2\pi}. \quad (16)$$

For the WBL, we can rewrite $\mathbf{T}^<(\varepsilon, -m, V)$ using the fact that $f(\varepsilon, \mu) + f(-\varepsilon, -\mu) = 1$. The electron density in Eq. (16) can thus be expressed as

$$\begin{aligned} \langle n_{k\bar{s}}(m, V) \rangle &= \int_{-\infty}^{\infty} (\mathbf{G}^- [\mathbf{\Gamma}_L(-m) + \mathbf{\Gamma}_R] \\ &\quad \times \mathbf{G}^+(\varepsilon, \langle n_{k\bar{s}}(m, V) \rangle, -m))_{ks,ks} \frac{d\varepsilon}{2\pi} \\ &\quad - \int_{-\infty}^{\infty} (\mathbf{G}^- \mathbf{T}_{\text{WBL}}^<(-\varepsilon, -m, -V) \\ &\quad \times \mathbf{G}^+(\varepsilon, \langle n_{k\bar{s}}(m, V) \rangle, -m))_{ks,ks} \frac{d\varepsilon}{2\pi}. \end{aligned} \quad (17)$$

From the properties of the HFA and HIA Green's functions, defined in Eqs. (7) and (8), it follows that they satisfy the identity $\mathbf{G}^- [\mathbf{\Gamma}_L + \mathbf{\Gamma}_R] \mathbf{G}^+ = \mathbf{G}^+ [\mathbf{\Gamma}_L + \mathbf{\Gamma}_R] \mathbf{G}^-$. This identity is used to rewrite the first term on the RHS, which is recognized to be equal to 1, because it can be interpreted as an electron density on site k with spin s , where the chemical potentials of the left and right leads are at infinity ($f(\varepsilon, \mu \rightarrow \infty) = 1$), yielding a filled level. Thus, this expression can be rewritten as

$$1 - \langle n_{k\bar{s}}(m, V) \rangle = \int_{-\infty}^{\infty} (\mathbf{G}^- \mathbf{T}_{\text{WBL}}^<(-\varepsilon, -m, -V) \times \mathbf{G}^+(\varepsilon, \langle n_{k\bar{s}}(m, V) \rangle, -m))_{ks,ks} \frac{d\varepsilon}{2\pi}. \quad (18)$$

Next, we use the bipartite lattice symmetry. First, we multiply the LHS and the RHS from the left and right with the matrix \mathbf{M} . The LHS does not change. On the RHS, we insert the identity matrix $\mathbf{I} = \mathbf{M}\mathbf{M}$ between the matrices of the product and finally use Eq. (12) to transform the Green's functions. The integration variable is changed as $\varepsilon \rightarrow -\varepsilon$ to obtain

$$1 - \langle n_{k\bar{s}}(m, V) \rangle = \int_{-\infty}^{\infty} (\mathbf{G}^+ \mathbf{T}_{\text{WBL}}^<(\varepsilon, -m, -V) \times \mathbf{G}^-(\varepsilon, 1 - \langle n_{k\bar{s}}(m, V) \rangle, -m))_{ks,ks} \frac{d\varepsilon}{2\pi}. \quad (19)$$

Note that Eq. (19) is, except for the density dependence of the Green's functions, almost the same as the expression for the densities $\langle n_{ks}(-m, -V) \rangle$:

$$\begin{aligned} \langle n_{ks}(-m, -V) \rangle &= \int_{-\infty}^{\infty} (\mathbf{G}^+ \mathbf{T}_{\text{WBL}}^<(\varepsilon, -m, -V) \\ &\quad \times \mathbf{G}^-(\varepsilon, \langle n_{ks}(-m, -V) \rangle, -m))_{ks,ks} \frac{d\varepsilon}{2\pi}. \end{aligned} \quad (20)$$

Equations (19) and (20) describe self-consistency equations for the respective densities. Self-consistent solutions of Eq. (20) are, by definition, solutions of Eq. (19) and vice versa. From this we conclude that

$$1 - \langle n_{k\bar{s}}(m, V) \rangle = \langle n_{ks}(-m, -V) \rangle. \quad (21)$$

Now, we turn to the magnetocurrent. The transmission is given by Eq. (5) and for WBL leads, the $\mathbf{\Gamma}_{L,R}$ is energy-independent. The time-reversal operator allows us to rewrite this expression as

$$T_{\text{LR}}(\varepsilon, m, V) = \text{Tr} [\mathbf{\Gamma}_L(m) \mathbf{G}^- \mathbf{\Gamma}_R \mathbf{G}^+(\varepsilon, \langle n_{k\bar{s}}(m, V) \rangle, -m)], \quad (22)$$

since $\mathbf{T}\langle n_{ks}(m, V) \rangle \mathbf{T}^{-1} = \langle n_{k\bar{s}}(m, V) \rangle$. The bipartite symmetry of the Green's function [Eq. (12)], in combination with $\langle n_{k\bar{s}}(m, V) \rangle = 1 - \langle n_{ks}(-m, -V) \rangle$ [Eq. (21)], implies

$$T_{\text{LR}}(\varepsilon, m, V) = \text{Tr} [\mathbf{\Gamma}_L(-m) \mathbf{G}^+ \mathbf{\Gamma}_R \mathbf{G}^-(-\varepsilon, \langle n_{ks}(-m, -V) \rangle, -m)]. \quad (23)$$

The expression on the RHS is recognized as the transmission for a negative magnetization and negative bias voltage and negative energy: $T_{\text{LR}}(-\varepsilon, -m, -V)$. Provided that the bias window is centered around the symmetric point $\varepsilon = 0$, it follows from the definition of the current [Eq. (4)] and this property of the transmission that

$$I(-m, -V) = -I(m, V). \quad (24)$$

Then, the magnetocurrent satisfies $\Delta I(m, V) = I(m, V) - I(-m, V) = I(m, -V) - I(-m, -V) = \Delta I(m, -V)$. Therefore, the magnetocurrent is a purely even function of the bias voltage $\Delta I_{\text{WBL}}(m, V) = \Delta I_{\text{WBL}}(m, -V)$.

E. Semi-Infinite leads

Here, we analyze the electron densities for SIF leads. First, we rewrite $\mathbf{T}^<(\varepsilon, m, V)$ using $f(\varepsilon, \mu) + f(-\varepsilon, -\mu) = 1$ and using Eq. (9) to rewrite $\mathbf{\Gamma}_L(\varepsilon, m)$ and $\mathbf{\Gamma}_R(\varepsilon)$. The electron density in Eq. (16) is then rewritten as

$$1 - \langle n_{k\bar{s}}(m, V) \rangle = \int_{-\infty}^{\infty} (\mathbf{G}^- \mathbf{T}_{\text{SIF}}^<(-\varepsilon, m, -V) \times \mathbf{G}^+(\varepsilon, \langle n_{k\bar{s}}(m, V) \rangle, -m))_{ks,ks} \frac{d\varepsilon}{2\pi}. \quad (25)$$

Note the opposite sign of the magnetization m in $\mathbf{T}_{\text{SIF}}^<$ in Eq. (25) with respect to that occurring in Eq. (18). Again, we apply the matrix \mathbf{M} to both sides and insert the identity matrix $\mathbf{I} = \mathbf{M}\mathbf{M}$ between the matrices of this product and use Eq. (13) to transform the Green's functions. Changing the integration variable as $\varepsilon \rightarrow -\varepsilon$ gives

$$1 - \langle n_{k\bar{s}}(m, V) \rangle = \int_{-\infty}^{\infty} (\mathbf{G}^+ \mathbf{T}_{\text{SIF}}^<(\varepsilon, m, -V) \times \mathbf{G}^-(\varepsilon, 1 - \langle n_{k\bar{s}}(m, V) \rangle, m))_{ks,ks} \frac{d\varepsilon}{2\pi}. \quad (26)$$

The RHS of this self-consistency equation has the same form as the one for $\langle n_{ks}(+m, -V) \rangle$. From this we conclude that

$$1 - \langle n_{k\bar{s}}(m, V) \rangle = \langle n_{ks}(m, -V) \rangle. \quad (27)$$

We now turn to the transmission, which is given by Eq. (5). For SIF leads, the $\Gamma_{L,R}$ is energy dependent. The Green's functions transform under time-reversal symmetry according to Eq. (11) and the transformation under bipartite lattice symmetry for semi-infinite leads according to Eq. (13). Combining these two transformations, we obtain for the transmission,

$$\begin{aligned} T_{LR}(\varepsilon, m, V) &= \text{Tr}[\Gamma_L(\varepsilon, -m)\mathbf{G}^+\Gamma_R(\varepsilon)\mathbf{G}^-(\varepsilon, 1 - \langle n_{k\bar{s}}(m, V) \rangle, m)], \\ &= \text{Tr}[\Gamma_L(-\varepsilon, m)\mathbf{G}^+\Gamma_R(-\varepsilon)\mathbf{G}^-(\varepsilon, \langle n_{ks}(m, -V) \rangle, m)], \\ &= T_{LR}(-\varepsilon, m, -V). \end{aligned} \quad (28)$$

In the last step, we rewrite $\Gamma_L(\varepsilon, -m)$ and $\Gamma_R(\varepsilon)$ using Eq. (9), and we use the assumption that the electron density satisfies Eq. (27). The RHS of Eq. (28) is recognized as the transmission for negative bias and negative energy. If the bias window is centered around the symmetric point $\varepsilon = 0$, then from the definition of the current Eqs. (4) and (28), it follows that $I(m, V) = -I(m, -V)$, and, thus, that the magnetocurrent is an odd function of bias voltage $\Delta I_{\text{SIF}}(m, V) = -\Delta I_{\text{SIF}}(m, -V)$. In Appendix B, we show that if the onsite energies of the left and right leads are equal to the chemical potential of the respective leads ($\varepsilon_{0,L} \rightarrow \mu_L = E_F + \frac{V}{2}$ and $\varepsilon_{0,R} \rightarrow \mu_R = E_F - \frac{V}{2}$), then still the magnetocurrent is an exactly odd function of bias voltage for SIF leads.

IV. NUMERICAL RESULTS

We use parameters corresponding to a molecule consisting of sp^2 -hybridized carbon atoms, to resemble the condition that we have one electron per site. The hopping parameter then is $t = 2.4$ eV,²⁸ and the onsite Coulomb interaction parameter $U_C = 10.06$ eV.²⁹ However, due to the image-charge effect,³⁰ the Coulomb interaction strength will be lowered to an extent, which sensitively depends on the molecule-lead separation. In our case, it is not known what the exact value of U will be due to the image-charge effect; probably we are in the regime where $U/t > 1$, making the HIA more appropriate. However, to show that our analytical result is independent of the approximation, we perform a numerical calculation for both the HFA and the HIA. We vary U between $0.5t$ and $3t$, where for small values of the Coulomb interaction strength ($U/t \leq 1$), the HFA is used, and, for large values ($U/t > 1$), the HIA is used. Furthermore, we take $T = 300$ K. The spin-orbit coupling parameter is taken to be $\lambda/t = 0.1$; this is rather large; however, we found that symmetry of the bias dependence of the magnetocurrent is not affected by the size λ . The magnitude of the magnetocurrent, of course, scales directly with λ . In the WBL, the coupling parameter to the leads is taken to be $\gamma_{L,R} = 0.5$ eV,²⁷ and $p_z^L = 0.5$. For SIF leads, the hopping parameter of the left and right leads is taken to be $t_{\text{lead}} = 3t$, the coupling parameter $t_{\text{coup}} = \frac{1}{2}\sqrt{t_{\text{lead}}}$, the magnetic polarization of the left lead is taken to be $p_z^L = 0.8$, and the onsite energies of the left and right leads are equal to the chemical potential of the respective leads ($\varepsilon_{0,L} \rightarrow \mu_L = \frac{V}{2}$ and $\varepsilon_{0,R} \rightarrow \mu_R = -\frac{V}{2}$). We always take the Fermi level $E_F = 0$. We have implemented a non-equilibrium transport code, which can be found in https://github.com/khhuisman/Coulomb_Bipartite.git, and for details regarding the calculation of the electron densities, see Appendix E.

In Figs. 2 and 3, the magnetocurrent is plotted as a function of bias voltage for leads in the WBL and Green's function in the

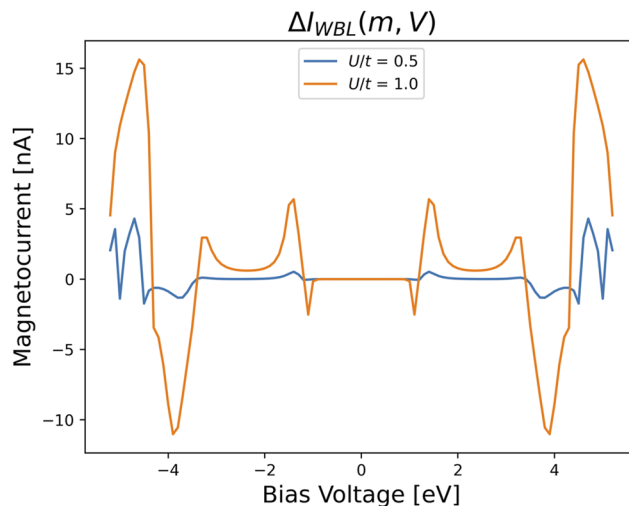


FIG. 2. The WBL magnetocurrent, $\Delta I_{\text{WBL}}(m, V)$, is plotted as a function of bias voltage in the HFA.

HFA and the HIA, respectively. Both figures show that the magnetocurrent is an even function of the bias voltage. This is explained as follows: We have found that the electron densities in the WBL satisfy Eq. (21), which we rewrite in the form

$$1 - \langle n_{k\bar{s}}(m, V) \rangle - \langle n_{ks}(-m, -V) \rangle = 0. \quad (29)$$

In our numerical calculations, we find that the LHS of this equation vanishes indeed (except for numerical errors that can be made small), which is due to the bipartite lattice symmetry of the Green's functions with WBL leads. In Sec. III D, we showed the magnetocurrent then is an even function of the bias voltage. We varied the

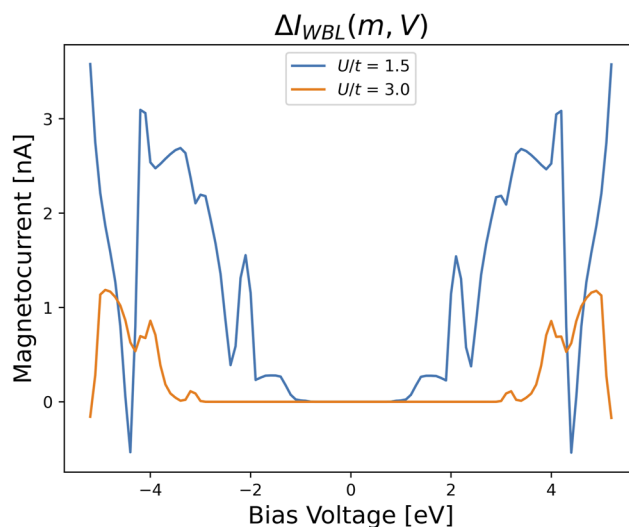


FIG. 3. The WBL magnetocurrent, $\Delta I_{\text{WBL}}(m, V)$, is plotted as a function of bias voltage in the HIA.

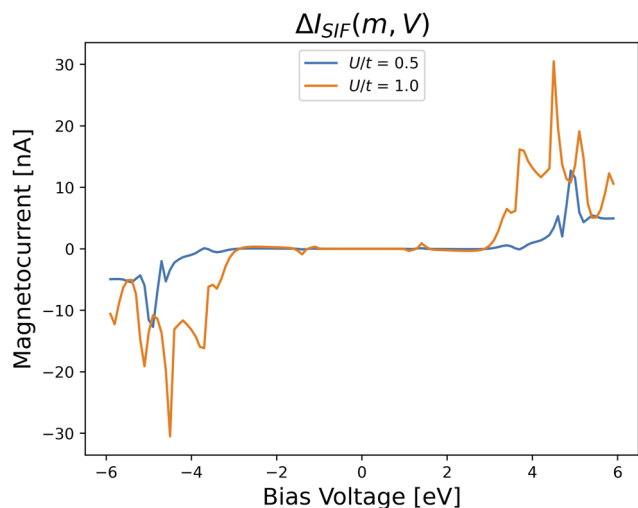


FIG. 4. The SIF magnetocurrent, $\Delta I_{\text{SIF}}(m, V)$, is plotted as a function of bias voltage in the HFA.

value of U/t for both the HFA and HIA and found that the magnetocurrent remained dominantly even. When an asymmetry between the coupling parameter to the left and right leads $\gamma_L \neq \gamma_R$ is introduced, the magnetocurrent remains a dominantly even function of bias voltage, as expected (see Appendix C). In Figs. 4 and 5, the magnetocurrent for SIF leads, $\Delta I_{\text{SIF}}(m, V)$, is plotted as a function of bias voltage for the HFA and the HIA, respectively. In both cases, the magnetocurrent is a dominantly odd function of bias voltage. We have found that the electron densities for SIF leads satisfy Eq. (27), which we rewrite in the form

$$1 - \langle n_{k\bar{s}}(m, V) \rangle - \langle n_{k\bar{s}}(m, -V) \rangle = 0. \quad (30)$$

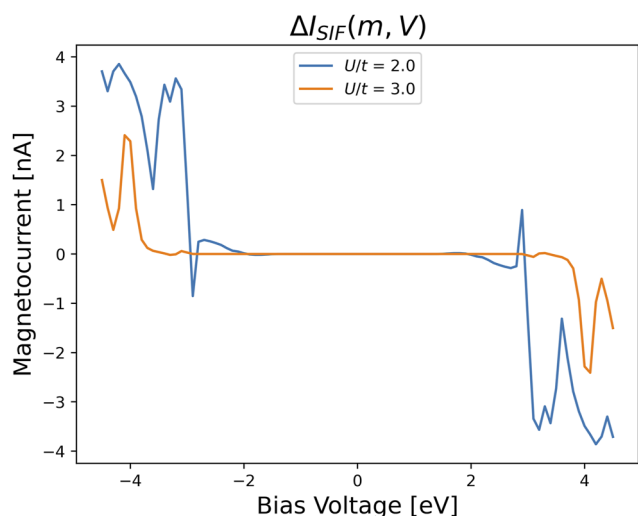


FIG. 5. The SIF magnetocurrent, $\Delta I_{\text{SIF}}(m, V)$, is plotted as a function of bias voltage in the HIA.

Again, we find in our numerical calculations, that the LHS of this equation vanishes. This is a consequence of the bipartite lattice symmetry of the Green's function with SIF leads and it explains why we find an odd magnetocurrent, as discussed in Sec. III E. Again, when an asymmetry in the coupling parameter t_c is introduced between the left and the right leads, we find that the magnetocurrent, as well as the odd function for SIF leads (see Appendix C) remains.

Finally, we demonstrate time-reversibility for the densities in equilibrium. As in our previous work on Coulomb interactions,²² our numerical results show that in equilibrium, the electron densities satisfy time-reversal symmetry $\langle n_{k\bar{s}}(m, V = 0) \rangle = \langle n_{k\bar{s}}(-m, V = 0) \rangle$, which is attributed to the Onsager–Casimir reciprocity. In Appendix D, we analytically show that the electron densities always satisfy time-reversal symmetry in equilibrium. Furthermore, we find that the magnetocurrent vanishes if the spin–orbit coupling parameter is set to zero and that the largest size of the effect, defined as $P_C = \frac{I(m) - I(-m)}{I(m) + I(-m)}$, is of the order 0.1%. A more minimal model of the S-shape (in Fig. 1), consisting of a chain with four sites and with a “kink” present between the second and the third sites, also shows a finite magnetocurrent that satisfies the same symmetries.

V. CONCLUSION

In this work, we studied the voltage dependence of the magnetocurrent for systems with Coulomb interactions (in the HFA and HIA) and a nearest neighbor spin–orbit coupling. We showed analytically that for a Fermi level that is aligned with energy around which the density of states is particle–hole symmetric and a capacitive coupling of the molecule to the lead that is symmetric, the magnetocurrent is exactly even in the WBL and exactly odd for SIF leads by exploiting the bipartite lattice symmetry of the Green's function. Our numerical calculations support this result. To test the predicted behavior of the magnetocurrent experimentally, a gate voltage can be used to align the energy around which the density of states is particle–hole symmetric with the Fermi-level. The WBL is appropriate for gold electrodes near the Fermi-level; thus, provided that the molecule is approximately particle–hole symmetric, an even magnetocurrent is expected. An asymmetry in the coupling from the molecule to the right and left leads ($\gamma_L \neq \gamma_R$) does not affect the symmetry properties either, as shown in Appendix C. In our previous work on Coulomb interactions,²² we modeled leads in the WBL, and we had a next-nearest neighbor spin–orbit coupling mechanism that destroys the bipartite lattice symmetry. When the Fermi level was aligned with the energy around which the density of states is approximately particle–hole symmetric and the capacitive coupling of the molecule to the lead that was symmetric, we found a nearly perfect odd magnetocurrent. The absence of bipartite lattice symmetry in our previous work is the reason why we find a behavior of the magnetocurrent different than that in this paper, where ΔI_{WBL} is even in bias voltage.

ACKNOWLEDGMENTS

This publication is part of the project “Chirality-induced spin selectivity” (with Project No. 680.92.18.01) of the research program “Natuurkunde Vrije Programma's,” which is financed by the Dutch Research Council (NWO).

AUTHOR DECLARATIONS

Conflict of Interest

The authors have no conflicts to disclose.

Author Contributions

K. H. Huisman: Data curation (equal); Investigation (equal); Software (equal); Writing – original draft (equal); Writing – review & editing (equal). **J. B. M. Y. Heinisch:** Data curation (equal); Investigation (equal); Writing – review & editing (equal). **J. M. Thijssen:** Supervision (equal); Writing – original draft (equal); Writing – review & editing (equal).

DATA AVAILABILITY

We have implemented a non-equilibrium transport code, which can be found in https://github.com/khhuisman/Coulomb_Bipartite.git.

APPENDIX A: GREEN'S FUNCTION: PARTICLE-HOLE TRANSFORMATION

In this section, we will show that the Hartree–Fock Green's function in Eq. (7) transforms as in Eqs. (12) and (13). In Eq. (7), the hopping matrices change sign under particle–hole transformation $\mathbf{M}\mathbf{H}_{\text{T,SOC}}\mathbf{M} = -\mathbf{H}_{\text{T,SOC}}$, while the self-energy $\Sigma(\epsilon, m)$ and the electron density matrix \mathbf{n} do not, because they are diagonal matrices $\mathbf{M}\Sigma(\epsilon, m)\mathbf{M} = \Sigma(\epsilon, m)$ and $\mathbf{M}\mathbf{n}\mathbf{M} = \mathbf{n}$ respectively. Therefore, in general, the HFA Green's function transforms as

$$\begin{aligned} & -\mathbf{M}\mathbf{G}_{\text{HFA}}^+(\epsilon, \langle n_{is}(m, V) \rangle, m)\mathbf{M} \\ &= -\left[\epsilon\mathbf{I} + \mathbf{H}_{\text{T}} + \mathbf{H}_{\text{SOC}} - U\mathbf{n} + \frac{U}{2}\mathbf{I} - \Sigma(\epsilon, m) \right]^{-1}, \\ &= \left[-\epsilon\mathbf{I} - \mathbf{H}_{\text{T}} - \mathbf{H}_{\text{SOC}} - U(\mathbf{I} - \mathbf{n}) + \frac{U}{2}\mathbf{I} + \Sigma(\epsilon, m) \right]^{-1}. \quad (\text{A1}) \end{aligned}$$

In the WBL, the retarded self-energy is purely imaginary and does not depend on energy $\Sigma(\epsilon, m) = -\frac{i}{2}\Gamma(m)$; therefore, $\Sigma(\epsilon, m) = -\Sigma^\dagger(-\epsilon, m)$. From this we obtain $-\mathbf{M}\mathbf{G}_{\text{HFA,WBL}}^+(\epsilon, \langle n_{is}(m, V) \rangle, m)\mathbf{M} = \mathbf{G}_{\text{HFA,WBL}}^-(-\epsilon, 1 - \langle n_{is}(m, V) \rangle, m)$.

For SIF leads, the retarded self-energy is given by $\Sigma(\epsilon, m) = \Lambda(\epsilon, m) - \frac{i}{2}\Gamma(\epsilon, m)$. In the region $|\epsilon - m| < 2t_{\text{lead}}$ Λ, Γ , it satisfies $\Lambda(\epsilon, m) = \frac{\epsilon - m}{2} = -\frac{-\epsilon - (-m)}{2} = -\Lambda(-\epsilon, -m)$ and $\Gamma(\epsilon, m) = \sqrt{(2t_{\text{lead}})^2 - (\epsilon - m)^2} = \Gamma(-\epsilon, -m)$. From this it follows that $\Sigma(\epsilon, m) = -\left[\Lambda(-\epsilon, -m) + \frac{i}{2}\Gamma(-\epsilon, -m) \right] = -\Sigma^\dagger(-\epsilon, -m)$. In the region $|\epsilon - m| \geq 2t_{\text{lead}}$, $\Gamma(\epsilon, m) = 0$; therefore, $\Sigma(\epsilon, m) = \frac{\epsilon - m}{2} - \text{sign}(\epsilon - m)\sqrt{(\epsilon - m)^2 - (2t_{\text{lead}})^2} = -\Lambda(-\epsilon, -m)^\dagger = -\Sigma^\dagger(-\epsilon, -m)$. In conclusion, for SIF leads, the reversal of the energy sign in the retarded self-energy is accompanied by a reversal of the magnetization and Hermitian conjugation $\Sigma(\epsilon, m) = \Sigma^\dagger(-\epsilon, -m)$, which leads to the relation $-\mathbf{M}\mathbf{G}_{\text{HFA,SIF}}^+(\epsilon, \langle n_{is}(m, V) \rangle, m)\mathbf{M} = \mathbf{G}_{\text{HFA,SIF}}^-(-\epsilon, 1 - \langle n_{is}(m, V) \rangle, -m)$. One can also show these relations for the Green's function in the Hubbard One approximation.

APPENDIX B: SEMI-INFINITE LEADS: VOLTAGE DEPENDENCE OF THE ONSITE ENERGY

In order to keep leads charge-neutral, the onsite energy of the lead shifts with the bias voltage such that $\epsilon_{0,L} = E_{\text{F}} + \frac{V}{2}$ and $\epsilon_{0,R} = E_{\text{F}} - \frac{V}{2}$. The retarded Green's function becomes explicitly voltage dependent via the retarded self-energy $\Sigma(\epsilon, m) \rightarrow \Sigma(\epsilon, m, V)$. Since we use the convention that $E_{\text{F}} = 0$, it follows from the properties of SIF leads (see Sec. III B) that Γ, Λ now satisfy

$$\Gamma(\epsilon, V, m) = \Gamma(-\epsilon, -V, -m), \quad (\text{B1})$$

$$\Lambda(\epsilon, V, m) = -\Lambda(-\epsilon, -V, -m), \quad (\text{B2})$$

where $\Gamma(\epsilon, V, m) = \sqrt{(2t_{\text{lead}})^2 - (\epsilon - m - \frac{V}{2})^2}$ and $\Lambda(\epsilon, V, m) = \frac{\epsilon - m - \frac{V}{2}}{2}$ for $|\epsilon - m - \frac{V}{2}| < 2t_{\text{lead}}$ and $\Gamma(\epsilon, V, m) = 0$, and $\Lambda(\epsilon, V, m) = \frac{\epsilon - m - \frac{V}{2}}{2} - \frac{1}{2}\text{sign}(\epsilon - m - \frac{V}{2})\sqrt{(\epsilon - m - \frac{V}{2})^2 - (2t_{\text{lead}})^2}$ for $|\epsilon - m - \frac{V}{2}| \geq 2t_{\text{lead}}$. Due to the properties in Eqs. (B1) and (B2), the bipartite lattice transformation for Green's functions now becomes

$$\begin{aligned} & \mathbf{G}_{\text{SIF}}^\pm(\epsilon, \langle n_{ks}(m, V) \rangle, m, V) \\ &= -\mathbf{M}\mathbf{G}_{\text{SIF}}^\mp(-\epsilon, 1 - \langle n_{ks}(m, V) \rangle, -m, -V)\mathbf{M}. \quad (\text{B3}) \end{aligned}$$

Note that in Eq. (B3), we added an explicit argument for the bias voltage V to indicate that the self-energy is voltage dependent.

The electron densities Eq. (14) are now given by

$$\langle n_{ks}(m, V) \rangle = \int (\mathbf{G}^+ \bar{\Gamma}_{\text{SIF}}^<(\epsilon, m, V) \mathbf{G}^-(\epsilon, \langle n_{ks}(m, V) \rangle, m, V))_{ks,ks} \frac{d\epsilon}{2\pi}, \quad (\text{B4})$$

where (for $E_{\text{F}} = 0$)

$$\bar{\Gamma}_{\text{SIF}}^<(\epsilon, m, V) = \Gamma_{\text{L}}(\epsilon, V, m) f\left(\epsilon, \frac{V}{2}\right) + \Gamma_{\text{R}}(\epsilon, V) f\left(\epsilon, -\frac{V}{2}\right). \quad (\text{B5})$$

Note that $\Gamma_{\text{L,R}}$ is voltage dependent quantities here. We use the time-reversal operator to rewrite Eq. (B4) as

$$\begin{aligned} \langle n_{k\bar{s}}(m, V) \rangle &= \int_{-\infty}^{\infty} (\mathbf{G}^- \bar{\Gamma}^<(\epsilon, -m, V) \\ &\times \mathbf{G}^+(\epsilon, \langle n_{k\bar{s}}(m, V) \rangle, -m, V))_{ks,ks} \frac{d\epsilon}{2\pi}. \quad (\text{B6}) \end{aligned}$$

Now, we rewrite $\bar{\Gamma}^<(\epsilon, -m, V)$ by using the fact that $f(\epsilon, \mu) + f(-\epsilon, -\mu) = 1$ and that $\Gamma_{\text{L}}(\epsilon, m, V)$ and $\Gamma_{\text{R}}(\epsilon, V)$ transform as in Eq. (B1). Analogous to Sec. III E, the electron density in Eq. (B6) is then rewritten as

$$\begin{aligned} 1 - \langle n_{k\bar{s}}(m, V) \rangle &= \int_{-\infty}^{\infty} (\mathbf{G}^- \bar{\Gamma}_{\text{SIF}}^<(-\epsilon, m, -V) \\ &\times \mathbf{G}^+(\epsilon, \langle n_{k\bar{s}}(m, V) \rangle, -m, V))_{ks,ks} \frac{d\epsilon}{2\pi}. \quad (\text{B7}) \end{aligned}$$

We then use the bipartite lattice symmetry. First, we multiply the LHS and the RHS from the left and right with the matrix \mathbf{M} , respectively. The LHS does not change. On the RHS, we insert the identity matrix $\mathbf{I} = \mathbf{M}\mathbf{M}$ between the matrices of this product and use

Eq. (B3) to transform the Green's functions. The integration variable changes as $\varepsilon \rightarrow -\varepsilon$ to obtain

$$1 - \langle n_{k\bar{s}}(m, V) \rangle = \int_{-\infty}^{\infty} (\mathbf{G}^+ \bar{\Gamma}_{\text{SIF}}^<(\varepsilon, m, -V) \times \mathbf{G}^-(\varepsilon, 1 - \langle n_{k\bar{s}}(m, V) \rangle, m, -V))_{ks,ks} \frac{d\varepsilon}{2\pi}. \quad (\text{B8})$$

Equation (B8) is identical to the self-consistency equation of $\langle n_{k\bar{s}}(+m, -V) \rangle$. From this we conclude that

$$1 - \langle n_{k\bar{s}}(m, V) \rangle = \langle n_{k\bar{s}}(m, -V) \rangle. \quad (\text{B9})$$

We now turn to the transmission, which is given by Eq. (5) and for SIF leads, $\Gamma_{L,R}$ is energy dependent. The Green's functions transform under time-reversal symmetry, as in Eq. (11), and the transformation under particle hole-symmetry for semi-infinite leads, as in Eq. (13). Combining these two transformations on the transmission, we obtain

$$T_{LR}(\varepsilon, m, V) = \text{Tr} \left[\Gamma_L(\varepsilon, -m, V) \mathbf{G}^+ \Gamma_R(\varepsilon, V) \times \mathbf{G}^-(\varepsilon, 1 - \langle n_{k\bar{s}}(m, V) \rangle, m, -V) \right]. \quad (\text{B10})$$

We then use Eq. (B1) to rewrite $\Gamma_L(\varepsilon, -m, V)$ and $\Gamma_R(\varepsilon, V)$ and find that the electron density satisfies Eq. (B9), to obtain $\text{Tr} \left[\Gamma_L(-\varepsilon, m, -V) \mathbf{G}^+ \Gamma_R(-\varepsilon, -V) \mathbf{G}^-(\varepsilon, \langle n_{k\bar{s}}(m, -V) \rangle, m, -V) \right]$, which is recognized as the transmission for negative bias negative energy. Thus, we conclude that

$$T_{LR}(\varepsilon, m, V) = T_{LR}(-\varepsilon, m, -V). \quad (\text{B11})$$

If the bias window is centered around the energy $\varepsilon = 0$, from the definition of the current, Eqs. (4) and (B11), it follows that $I(m, V) = -I(m, -V)$, and, thus, that the magnetocurrent is an odd function of bias voltage $\Delta I_{\text{SIF}}(m, V) = -\Delta I_{\text{SIF}}(m, -V)$.

APPENDIX C: ASYMMETRIC COUPLING

In the molecular junction, there is often an asymmetry in the coupling of the molecule to the left and right leads i.e., $\gamma_L \neq \gamma_R$. In the wide-band limit, we quantify this asymmetry by introducing the dimensionless parameter $\chi = \frac{\gamma_L - \gamma_R}{\gamma_L + \gamma_R}$. In Fig. 6, the wide-band limit magnetocurrent is plotted as a function of bias voltage for different values of this parameter $\chi = -0.6, 0, 0.6$ [corresponding to $(\gamma_L, \gamma_R) = (0.5, 2), (0.5, 0.5), (2, 0.5)$, respectively], in the HFA for $U = 2t, p_z = 0.5$. It clearly shows that the magnetocurrent is an even function of bias voltage, independent of the value of χ .

For SIF leads, we quantify this asymmetry by introducing the dimensionless parameter $\chi_2 = \frac{t_c^L - t_c^R}{t_c^L + t_c^R}$, where t_c^α is the coupling parameter for electrons on the molecule on electrons on lead α . In Fig. 7, the SIF magnetocurrent is plotted as a function of bias voltage for $p_z = 0.8, t_{\text{lead}}^{L,R} = 2t, t_c^R = \frac{1}{2}\sqrt{t_{\text{lead}}^R}, t_c^L = 2\sqrt{t_{\text{lead}}^L}$ and $\frac{U}{t} = 0.5, 1$ in the HFA. The figure shows that the magnetocurrent remains an odd function of voltage. For the HIA, the magnetocurrent remains an even function of bias voltage in the WBL and an odd function of bias voltage for SIF leads, when an asymmetry in the coupling constant is introduced.

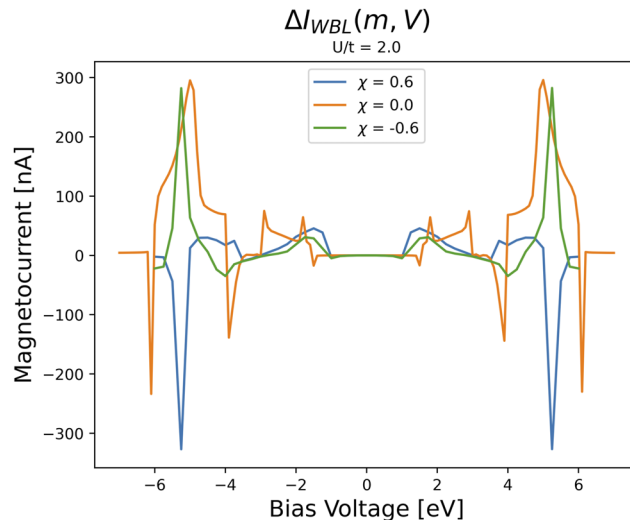


FIG. 6. The magnetocurrent in the HFA is plotted as a function of bias voltage when an asymmetry between the coupling in the left and right leads is introduced for WBL leads.

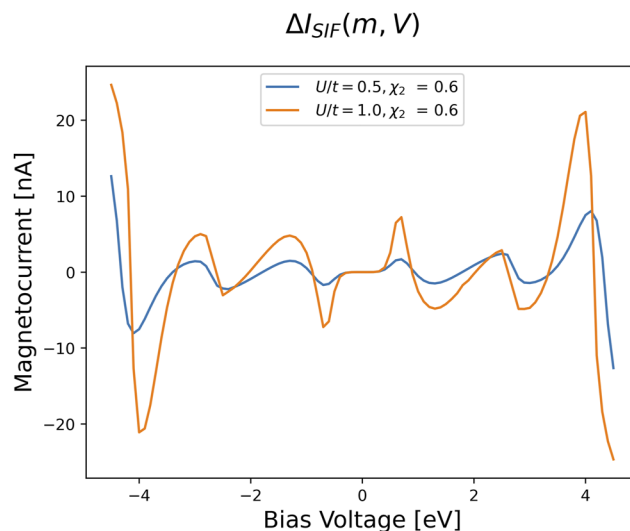


FIG. 7. The magnetocurrent in the HFA is plotted as a function of bias voltage when an asymmetry between the coupling in the left and right leads is introduced for SIF leads.

APPENDIX D: TIME-REVERSAL SYMMETRY IN EQUILIBRIUM

Here, we show analytically that in equilibrium, the electron densities satisfy time-reversal symmetry. To be unambiguous, we define equilibrium as $V = 0$ (i.e., $\mu_L = \mu_R$) and take equal temperatures for both leads (i.e., $T_L = T_R$); if one of these conditions is vio-

lated, we say that the system is out of equilibrium.³¹ In equilibrium, the electron density [Eq. (14)] is given by

$$\langle n_{k\bar{s}}(m, V = 0) \rangle = \int_{-\infty}^{\infty} f_0(\mathbf{G}^+[\Gamma_L + \Gamma_R] \times \mathbf{G}^-(\varepsilon, \langle n_{k\bar{s}}(m, V = 0) \rangle, m))_{k\bar{s},k\bar{s}} \frac{d\varepsilon}{2\pi}, \quad (\text{D1})$$

where we define $f_0 = f_{L,R}(E)|_{V=0} = [\exp(\beta(E - E_F)) + 1]^{-1}$. From the time-reversal property of the Green's function Eq. (11) and $\mathbf{T}\langle n_{k\bar{s}}(m, V = 0) \rangle \mathbf{T}^{-1} = \langle n_{k\bar{s}}(m, V = 0) \rangle$, follows the identity $\mathbf{G}^+[\Gamma_L + \Gamma_R]\mathbf{G}^-(\varepsilon, \mathbf{n}_s(m, V = 0), m) = \mathbf{T}^{-1}\mathbf{G}^-[\Gamma_L + \Gamma_R]\mathbf{G}^+(\varepsilon, \mathbf{n}_{\bar{s}}(m, V = 0), -m)\mathbf{T}$, which we use to rewrite the RHS of Eq. (D1). We then multiply both sides from the left with \mathbf{T} and from the right with \mathbf{T}^{-1} , which flips the spin on the LHS and cancels the time-reversal operators on the RHS. We then use the identity $\mathbf{G}^-[\Gamma_L + \Gamma_R]\mathbf{G}^+ = \mathbf{G}^+[\Gamma_L + \Gamma_R]\mathbf{G}^-$, which follows from the definition of the Green's functions in Eqs. (7) and (8), to rewrite the RHS, and we obtain

$$\langle n_{k\bar{s}}(m, V = 0) \rangle = \int_{-\infty}^{\infty} f_0(\mathbf{G}^+[\Gamma_L + \Gamma_R] \times \mathbf{G}^-(\varepsilon, \langle n_{k\bar{s}}(m, V = 0) \rangle, -m))_{k\bar{s},k\bar{s}} \frac{d\varepsilon}{2\pi}. \quad (\text{D2})$$

The self-consistency equation above in Eq. (D2) is the same as the self-consistency equation of $\langle n_{k\bar{s}}(-m, V = 0) \rangle$. Therefore, we obtain the relation

$$\langle n_{k\bar{s}}(m, V = 0) \rangle = \langle n_{k\bar{s}}(-m, V = 0) \rangle. \quad (\text{D3})$$

which is recognized as the time-reversal symmetry in equilibrium since both spin and magnetization change sign. In our previous work on Coulomb interactions,²² we showed that time-reversal symmetry in equilibrium leads to the fulfillment of the Onsager–Casimir reciprocity. Note that this conclusion holds for bipartite and non-bipartite lattices and also holds for any value of Fermi level E_F .

Perhaps it seems like a circular argument presented here since we use the time-reversal operator to prove that time-reversal symmetry is satisfied in equilibrium. However, no such circular argument is presented. If the temperatures in the left and right leads are unequal (i.e., out of equilibrium), the electron densities, after applying the time-reversal operator left and right, become

$$\langle n_{k\bar{s}}(m, V = 0) \rangle = \int_{-\infty}^{\infty} (\mathbf{G}^-[\Gamma_L f_L + \Gamma_R f_R] \times \mathbf{G}^+(\varepsilon, \langle n_{k\bar{s}}(m, V = 0) \rangle, -m))_{k\bar{s},k\bar{s}} \frac{d\varepsilon}{2\pi}. \quad (\text{D4})$$

Note that the Green's functions here are reversed with respect to the ones in Eq. (D1). Before, we could use the identity $\mathbf{G}^-[\Gamma_L + \Gamma_R]\mathbf{G}^+ = \mathbf{G}^+[\Gamma_L + \Gamma_R]\mathbf{G}^-$. However, in this case, we cannot reverse the Green's functions since $\mathbf{G}^-[\Gamma_L f_L + \Gamma_R f_R]\mathbf{G}^+ \neq \mathbf{G}^+[\Gamma_L f_L + \Gamma_R f_R]\mathbf{G}^-$ and, therefore, $\langle n_{k\bar{s}}(m, V = 0) \rangle \neq \langle n_{k\bar{s}}(-m, V = 0) \rangle$. Therefore, we conclude that for unequal temperatures in the left and right leads (i.e., “out of equilibrium”), the electron densities do not satisfy this time reversal property, consistent with our numerical calculations, which show a very small deviation from TRS in that case and a linear magnetocurrent in that case.

APPENDIX E: SELF-CONSISTENT DETERMINATION OF THE ELECTRON DENSITIES

In our transport code, we determine the electron density as follows: Suppose we want to calculate the electron density for the decreasing or increasing bias voltages $\{0, V_1, V_2, \dots\}$, ($|V_{i+1}| > |V_i|$). First of all, we start our self-consistent calculation at zero bias voltage, where we expect that every site is approximately half-filled; therefore, we take this as an initial guess ($\langle n_{k\bar{s}}^{in,m=0}(V = 0) \rangle = \frac{1}{2}$). Then, we self-consistently determine the electron densities for $V = 0$ and obtain the converged result $\langle n_{k\bar{s}}^{converged}(V = 0) \rangle$. We then use these values as an initial guess for the next bias voltage V_1 , $\langle n_{k\bar{s}}^{in,m=0}(V = V_1) \rangle = \langle n_{k\bar{s}}^{converged}(V = 0) \rangle$. We always use the output of a self-consistent calculation as the initial guess for the next bias voltage $\langle n_{k\bar{s}}^{in,m=0}(V = V_{i+1}) \rangle = \langle n_{k\bar{s}}^{converged}(V = V_i) \rangle$ to adiabatically connect the two solutions. This procedure is done separately for positive and negative biases and both times we start in $V = 0$. Now follows a description of a self-consistent loop for bias voltage V_i . Given an initial guess for bias voltage V_i we iterate over Eq. (14), m_{\max} times. Every iteration m has an input and an output electron density and as convergence criterion for the m th iteration, we use $|\langle n_{k\bar{s}}^{in,m} \rangle - \langle n_{k\bar{s}}^{out,m} \rangle| < 10^{-4}$. If a density did not converge within the maximum number of iterations m_{\max} , we discard it. Furthermore, we employ linear mixing of the electron densities, meaning that the input for iteration $m + 1$ is a linear combination of the input and output of iteration m , $\langle n_{k\bar{s}}^{in,m+1}(V_i) \rangle = (1 - \alpha)\langle n_{k\bar{s}}^{out,m}(V_i) \rangle + \alpha\langle n_{k\bar{s}}^{in,m}(V_i) \rangle$, characterized by the parameter $\alpha \in [0, 1]$.

The Hamiltonian of the isolated molecule, without interactions ($U = 0$), is defined as $\mathbf{H}_0 = \mathbf{H}_T + \mathbf{H}_{\text{SOC}}$ and is constructed with the Kwant code³² and the Qsymm code.³³

APPENDIX F: FORMULA FOR THE CURRENT

In the work of Meir and Wingreen,³⁴ the current into the left lead is given by their Eq. (5):

$$I_L = \frac{ie}{h} \int \text{Tr}[\Gamma_L(\varepsilon)[f(\varepsilon, \mu_L)(\mathbf{G}^+(\varepsilon) - \mathbf{G}^-(\varepsilon)) + \mathbf{G}^<(\varepsilon)]]d\varepsilon. \quad (\text{F1})$$

We now show that $\mathbf{G}^+(\varepsilon) - \mathbf{G}^-(\varepsilon) = -i\mathbf{G}^+(\varepsilon)(\Gamma_L(\varepsilon) + \Gamma_R(\varepsilon))\mathbf{G}^-(\varepsilon)$ in the HIA. Let us first rewrite $\mathbf{G}^{\pm}(\varepsilon)$ in Eq. (8):

$$\mathbf{G}^+(\varepsilon) = \frac{1}{\mathbf{g}_0(\varepsilon)^{-1} - \Sigma(\varepsilon)}, \quad \mathbf{G}^-(\varepsilon) = \frac{1}{(\mathbf{g}_0(\varepsilon)^\dagger)^{-1} - \Sigma^\dagger(\varepsilon)}, \quad (\text{F2})$$

where we define: $\mathbf{g}_0(\varepsilon)^{-1} = [(\varepsilon - \frac{U}{2})\mathbf{I} + U\mathbf{n}]^{-1}(\varepsilon - \frac{U}{2})(\varepsilon + \frac{U}{2})\mathbf{I} - \mathbf{H}_T - \mathbf{H}_{\text{SOC}}$, where the matrix \mathbf{n} has elements $n_{k\bar{s},k'\bar{s}'} = \langle n_{k\bar{s}} \rangle \delta_{kk'} \delta_{\bar{s}\bar{s}'}$ (where \bar{s} denotes that spin s is flipped). Consequently, $\mathbf{G}^+(\varepsilon) - \mathbf{G}^-(\varepsilon) = \mathbf{G}^+(\varepsilon)(\Sigma(\varepsilon) - \Sigma^\dagger(\varepsilon) + (\mathbf{g}_0(\varepsilon)^\dagger)^{-1} - \mathbf{g}_0(\varepsilon)^{-1})\mathbf{G}^-(\varepsilon)$. Since $\mathbf{g}_0(\varepsilon)$ contains no anti-Hermitian parts, $\mathbf{g}_0(\varepsilon)$ is a Hermitian matrix. Here, $\Sigma(\varepsilon) = \Sigma_L(\varepsilon) + \Sigma_R(\varepsilon)$ is the usual retarded self-energy of the leads, and $\Gamma_{L,R}(\varepsilon) = -i(\Sigma_{L,R}(\varepsilon) - \Sigma_{L,R}(\varepsilon)^\dagger)$. Consequently, $\mathbf{G}^+(\varepsilon) - \mathbf{G}^-(\varepsilon) = -i\mathbf{G}^+(\varepsilon)(\Gamma_L(\varepsilon) + \Gamma_R(\varepsilon))\mathbf{G}^-(\varepsilon)$ in the HIA.

Equation (F1) reduces to the Landauer–Büttiker formula in the case that the lesser Green's function is given by $\mathbf{G}^<(\varepsilon) = i\mathbf{G}^+(\varepsilon)(\Gamma_L(\varepsilon)f(\varepsilon, \mu_L) + \Gamma_R(\varepsilon)f(\varepsilon, \mu_R))\mathbf{G}^-(\varepsilon)$ and the retarded

and advanced Green's functions are related as $G^+(\varepsilon) - G^-(\varepsilon) = -iG^+(\varepsilon)(\Gamma_L(\varepsilon) + \Gamma_R(\varepsilon))G^-(\varepsilon)$. We always assume this expression for the lesser Green's function. The latter expression holds for the HFA and HIA, justifying the use of the Landauer–Büttiker formula.

In the analysis of the electron–phonon coupling, the Lang–Firsov transformation is usually applied.³⁵ This induces a coupling between the vibrational system on the molecule and the leads, preventing us from requiring the leads to be in equilibrium, which is necessary for writing Eq. (F1).

REFERENCES

- 1 L. Onsager, "Reciprocal relations in irreversible processes. I," *Phys. Rev.* **37**, 405–426 (1931).
- 2 L. Onsager, "Reciprocal relations in irreversible processes. II," *Phys. Rev.* **38**, 2265–2279 (1931).
- 3 H. B. G. Casimir, "On Onsager's principle of microscopic reversibility," *Rev. Mod. Phys.* **17**, 343–350 (1945).
- 4 M. Büttiker, "Symmetry of electrical conduction," *IBM J. Res. Dev.* **32**, 317–334 (1988).
- 5 C. Kulkarni, A. K. Mondal, T. K. Das, G. Grinbom, F. Tassinari, M. F. J. Mabesoone, E. W. Meijer, and R. Naaman, "Highly efficient and tunable filtering of electrons' spin by supramolecular chirality of nanofiber-based materials," *Adv. Mater.* **32**, 1904965 (2020).
- 6 H. Lu, C. Xiao, R. Song, T. Li, A. E. Maughan, A. Levin, R. Brunecky, J. J. Berry, D. B. Mitzi, V. Blum, and M. C. Beard, "Highly distorted chiral two-dimensional tin iodide perovskites for spin polarized charge transport," *J. Am. Chem. Soc.* **142**, 13030–13040 (2020).
- 7 U. Huizi-Rayo, J. Gutierrez, J. M. Seco, V. Mujica, I. Diez-Perez, J. M. Ugalde, A. Tercjak, J. Cepeda, and E. San Sebastian, "An ideal spin filter: Long-range, high-spin selectivity in chiral helicoidal 3-dimensional metal organic frameworks," *Nano Lett.* **20**, 8476–8482 (2020).
- 8 H. Al-Bustami, G. Koplovitz, D. Primc, S. Yochelis, E. Capua, D. Porath, R. Naaman, and Y. Paltiel, "Single nanoparticle magnetic spin memristor," *Small* **14**, 1801249 (2018).
- 9 G. Koplovitz, D. Primc, O. Ben Dor, S. Yochelis, D. Rotem, D. Porath, and Y. Paltiel, "Magnetic nanoplatelet-based spin memory device operating at ambient temperatures," *Adv. Mater.* **29**, 1606748 (2017).
- 10 T. Liu, X. Wang, H. Wang, G. Shi, F. Gao, H. Feng, H. Deng, L. Hu, E. Lochner, P. Schlottmann, S. von Molnár, Y. Li, J. Zhao, and P. Xiong, "Linear and nonlinear two-terminal spin-valve effect from chirality-induced spin selectivity," *ACS Nano* **14**, 15983–15991 (2020).
- 11 M. W. Rahman, S. Firouzeh, and S. Pramanik, "Carrier localization and magnetoresistance in DNA-functionalized carbon nanotubes," *Nanotechnology* **32**, 455001 (2021).
- 12 V. Kiran, S. P. Mathew, S. R. Cohen, I. Hernández Delgado, J. Lacour, and R. Naaman, "Helicenes—A new class of organic spin filter," *Adv. Mater.* **28**, 1957 (2016).
- 13 Z. Xie, T. Z. Markus, S. R. Cohen, Z. Vager, R. Gutierrez, and R. Naaman, "Correction to spin specific electron conduction through DNA oligomers," *Nano Lett.* **12**, 523 (2012).
- 14 G. Bullard, F. Tassinari, C.-H. Ko, A. K. Mondal, R. Wang, S. Mishra, R. Naaman, and M. J. Therien, "Low-resistance molecular wires propagate spin-polarized currents," *J. Am. Chem. Soc.* **141**, 14707–14711 (2019).
- 15 F. Tassinari, D. R. Jayarathna, N. Kantor-Uriel, K. L. Davis, V. Varade, C. Achim, and R. Naaman, "Chirality dependent charge transfer rate in oligopeptides," *Adv. Mater.* **30**, 1706423 (2018).
- 16 B. P. Bloom, V. Kiran, V. Varade, R. Naaman, and D. H. Waldeck, "Spin selective charge transport through cysteine capped CdSe quantum dots," *Nano Lett.* **16**, 4583–4589 (2016).
- 17 T. N. H. Nguyen, L. Rasabathina, O. Hellwig, A. Sharma, G. Salvan, S. Yochelis, Y. Paltiel, L. T. Baczewski, and C. Tegenkamp, "Cooperative effect of electron spin polarization in chiral molecules studied with non-spin-polarized scanning tunneling microscopy," *ACS Appl. Mater. Interfaces* **14**, 38013–38020 (2022).
- 18 C. D. Aiello, J. M. Abendroth, M. Abbas, A. Afanasev, S. Agarwal, A. S. Banerjee, D. N. Beratan, J. N. Belling, B. Berche, A. Botana, J. R. Caram, G. L. Celardo, G. Cuniberti, A. Garcia-Etxarri, A. Dianat, I. Diez-Perez, Y. Guo, R. Gutierrez, C. Herrmann, J. Hihath, S. Kale, P. Kurian, Y.-C. Lai, T. Liu, A. Lopez, E. Medina, V. Mujica, R. Naaman, M. Noormandipour, J. L. Palma, Y. Paltiel, W. Petuskey, J. C. Ribeiro-Silva, J. J. Saenz, E. J. G. Santos, M. Solyanik-Gorgone, V. J. Sorger, D. M. Stemer, J. M. Ugalde, A. Valdes-Curiel, S. Varela, D. H. Waldeck, M. R. Wasielewski, P. S. Weiss, H. Zacharias, and Q. H. Wang, "A chirality-based quantum leap," *ACS Nano* **16**, 4989–5035 (2022).
- 19 X. Yang, C. H. van der Wal, and B. J. van Wees, "Detecting chirality in two-terminal electronic nanodevices," *Nano Lett.* **20**, 6148–6154 (2020).
- 20 K. H. Huisman and J. M. Thijssen, "CISS effect: A magnetoresistance through inelastic scattering," *J. Phys. Chem. C* **125**, 23364–23369 (2021).
- 21 T. K. Das, F. Tassinari, R. Naaman, and J. Fransson, "Temperature-dependent chiral-induced spin selectivity effect: Experiments and theory," *J. Phys. Chem. C* **126**, 3257–3264 (2022).
- 22 K. H. Huisman, J.-B. M.-Y. Heinisch, and J. M. Thijssen, "Chirality-induced spin selectivity (CISS) effect: Magnetocurrent–voltage characteristics with Coulomb interactions. I," *J. Phys. Chem. C* **127**, 6900–6905 (2023).
- 23 M. Rebergen, "A study of induced spin selectivity in chiral molecules," M.S. thesis, Delft University of Technology, 2018.
- 24 J. Fransson, "Chirality-induced spin selectivity: The role of electron correlations," *J. Phys. Chem. Lett.* **10**, 7126–7132 (2019).
- 25 A.-P. Jauho and H. Haug, *Quantum Kinetics in Transport and Optics of Semiconductors* (Springer, 2008).
- 26 D. M. Newns, "Self-consistent model of hydrogen chemisorption," *Phys. Rev.* **178**, 1123–1135 (1969).
- 27 C. J. O. Verzijl, J. S. Seldenthuis, and J. M. Thijssen, "Applicability of the wide-band limit in DFT-based molecular transport calculations," *J. Chem. Phys.* **138**, 094102 (2013).
- 28 S. Ramasesha, B. Sinha, and I. D. L. Albert, "Nature of exchange interactions in stacked radicals/radical-ions of cyclic polyenes," *J. Mol. Struct.* **327**, 173–180 (1994).
- 29 R. J. Bursill, C. Castleton, and W. Barford, "Optimal parametrisation of the Pariser–Parr–Pople model for benzene and biphenyl," *Chem. Phys. Lett.* **294**, 305–313 (1998).
- 30 C. J. O. Verzijl, J. A. C. Gil, M. L. Perrin, D. Dulić, H. S. J. van der Zant, and J. M. Thijssen, "Image effects in transport at metal–molecule interfaces," *J. Chem. Phys.* **143**, 174106 (2015).
- 31 P. A. Jacquet, "Thermoelectric transport properties of a chain of quantum dots with self-consistent reservoirs," *J. Stat. Phys.* **134**, 709–748 (2009).
- 32 C. W. Groth, M. Wimmer, A. R. Akhmerov, and X. Waintal, "Kwant: A software package for quantum transport," *New J. Phys.* **16**, 063065 (2014).
- 33 D. Varjas, T. Ö. Rosdahl, and A. R. Akhmerov, "Qsymm: Algorithmic symmetry finding and symmetric Hamiltonian generation," *New J. Phys.* **20**, 093026 (2018).
- 34 Y. Meir and N. S. Wingreen, "Landauer formula for the current through an interacting electron region," *Phys. Rev. Lett.* **68**, 2512–2515 (1992).
- 35 M. Galperin, A. Nitzan, and M. A. Ratner, "Inelastic effects in molecular junctions in the Coulomb and Kondo regimes: Nonequilibrium equation-of-motion approach," *Phys. Rev. B* **76**, 035301 (2007).